Toward a More Complete Analysis for Fluid-Structure Interaction in Helicopters

KyungHwan Kim,* SangJoon Shin,**
School of Mechanical and Aerospace Engineering
Seoul National University, Seoul, Korea, 151-742

Jaewon Lee,* Kwanjung Yee,**** and Sejong Oh******
Department of Aerospace Engineering
Pusan National University, Pusan, Korea, 609-735

Abstract

There have been developed many structural and fluid rotorcraft analysis models in rotorcraft community, and also lots of investigations have been conducted to combine these two models. These investigations turn out to be good at predicting the airloads precisely, but they have not taken the blade nonlinear deflection into account. For this reason, the present paper adopts a sophisticated structural model which can describe three-dimensional nonlinear deflection of the blade. And it is combined with two types of aerodynamic model. First one is generalized Greenberg type of finite-time aerodynamic model, which is originally established for a fixed wing, but later modified to be suitable for coupled flap-lag-torsional aeroelastic analysis of the rotor blade. Second aerodynamic model is based on the unsteady source-doublet panel method coupled with a free wake model. The advantages of the present method are capabilities to consider thickness of the blade and more precise wake effects. Transient responses of the airloads and structural deflections in time domain are mainly analyzed in this paper.

Key Word : Rotor blade analysis, Geometrically nonlinear beam, Generalized Greenberg's theory, Unsteady source-doublet method, Fluid-structure interaction

Introduction

In a helicopter system that obtains lift, thrust, and control force by rotating blades, its blade structure exhibits complicated environment, which requires precise prediction of inertial, aerodynamic, elastic forces, etc. acting on it. The motion of blades results as a consequence of the interaction of these forces, and therefore an accurate estimation of such interaction is strongly required to predict the behavior of the rotor blade. Different from that of fixed-wing airplanes, rotary-wing aeroelasticity is affected by several unique and specific phenomena such as the followings. The advancing side experiences very fast airflow causing compressibility, while the retreating side experiences dynamic stall and reverse flow. Blade vortex interaction (BVI) is generated by interaction between the rotor blades and the strong tip vortices created by the

* Graduate Student
E-mail : sparky98@snu.ac.kr Tel : 02-880-1901 Fax : 02-887-2662
** Professor, Institute of Advanced Aerospace Technology
*** Graduate Student
**** Professor

preceding blades and becomes an important factor. All of these phenomena result in excessive noise and vibration upon the helicopter fuselage. Vibration induces fatigue problem in the helicopter components. Noise imposes severe limits upon operation in urban areas and restrictions on the pilot and passengers. To correctly understand and alleviate these problems, it has been requested an analytical capability for the interaction between structure and aerodynamics since the advent of helicopters.

There have been developed quite a few computational fluid dynamics (CFD) and computational structural dynamics (CSD) analyses in the rotorcraft community. Examples of these are CAMRAD II, UMARC, 2GCHAS, DYMORE and OVERFLOW-D, etc. Also a number of investigations to combine these two types of analyses have been conducted, such as Potsdam *et al.* [1] and Datta *et al.* [2]. These investigations turned out to be quite useful for improving accuracy of prediction, however they required considerable computational resources as well as computation time and model complicacy. They were not capable of taking the nonlinear deflection of blades into the analysis, either. With all these considerations, the present paper adopts finite-time and source-double aerodynamic model instead of a complicated CFD analysis and a sophisticated blade structural dynamics model.

To describe the motion of the rotor blade precisely which exhibits large deflection and moderate rotation, geometrical nonlinearity should be considered. In this paper, geometrical exactness is completely formulated to include the coupling between bending and torsion deformation. An exact intrinsic equation is utilized in the present approach, and it also requires cross-sectional properties. Geometrically nonlinear formulation of three-dimensional elasticity for a moving beam is separated into a nonlinear one-dimensional problem and a linear two-dimensional problem. The two-dimensional cross-sectional analysis adopts a variational asymptotic approach, taking into account of curvature, twist and warping effects, and is consistent with three-dimensional elasticity theory to obtain the cross-section stiffness constants for an anisotropic beam. In this paper, an existing analysis result on a certain experimental blade cross section based on a variational asymptotical approach [3] is used. In the one-dimensional analysis, mixed variational formulation based on exact intrinsic equations for dynamics of moving beams is used to compute the global deformation or response of the blade.

Two different aerodynamic models are adopted to deal with various rotor blade configurations. One is a generalized version of Greenberg theory [4] for case I, and the other is a source-doublet method [5] which can simulate more precise unsteady aerodynamics for case II.

Theoritical Modeling

Global frame and frame transformation

To apply the mixed variational formulation for dynamics of moving beams, it is necessary to introduce a global frame which is shown in Figure 1. The global frame named a, with its axes labeled a_1, a_2 and a_3 is rotating with the rotor at the predefined angular velocity. The undeformed

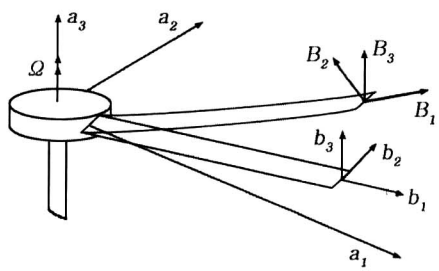

Fig. 1. Framesets used in the formulation for dynamics of moving beams

reference frame of blades is named b, with its axes labeled by b_1, b_2 and b_3. Its deformed reference frame is named B, with its axes expressed by B_1, B_2 and B_3.

Using the transformation matrices, transformation among the frames is enabled without destroying its compactness. For example, an arbitrary vector Z can be expressed by its components in frames of a, b or B, with their relations being

$$Z_a = C^{ba} Z_a \ , \quad Z_B = C^{Ba} Z_a \tag{1}$$

where C^{ba} is the transformation matrix from a to b, and C^{Ba} is that from a to B.

Structural model

For the blade structure modeling, mixed form of the variational equation is used [6]. The formulation is derived using Hamilton's principle and it can be written as

$$\int_{t_1}^{t_2} \int_0^l [\delta(K-U) + \overline{\delta W}] dx_1 dt = \overline{\delta A} \tag{2}$$

where t_1 and t_2 are arbitrary fixed times, l is the length of the beam, K and U are the kinetic and potential energy densities per unit length, respectively. $\overline{\delta A}$ is the virtual action at the ends of the beam and at the ends of the time interval, and $\overline{\delta W}$ is the virtual work of applied loads per unit length.

The variation of kinetic energy and potential terms is with respect to the column vectors of V_B, Ω_B, γ and κ, which are linear and angular velocity, force and momentum strain, respectively. The internal force and moment vectors F_B and M_B and linear and angular momentum vectors P_B and H_B are defined as

$$\begin{aligned} F_B &= \left(\frac{\partial U}{\partial \gamma}\right)^T , \quad M_B = \left(\frac{\partial U}{\partial \kappa}\right)^T \\ P_B &= \left(\frac{\partial K}{\partial V_B}\right)^T , \quad H_B = \left(\frac{\partial K}{\partial \Omega_B}\right)^T , \end{aligned} \tag{3}$$

The generalized strain and force measure, and velocity and momentum measures are related through the constitutive laws in the following form:

$$\begin{Bmatrix} F_B \\ M_B \end{Bmatrix} = [S] \begin{Bmatrix} \gamma \\ \kappa \end{Bmatrix} \ , \quad \begin{Bmatrix} P_B \\ H_B \end{Bmatrix} = \begin{bmatrix} m\Delta & 0 \\ 0 & I \end{bmatrix} \begin{Bmatrix} V_B \\ \Omega_B \end{Bmatrix} \tag{4}$$

where $[S]$ is 6×6 stiffness matrix, m is the mass density per unit length, and I is the matrix of moment of inertia.

With the above equations, equation (2) can be written as

$$\int_{t_1}^{t_2} \int_0^l \left[\delta V_B^{*T} P_B + \delta \Omega_B^{*T} H_B - \delta \gamma^{*T} F_B - \delta \gamma^{*T} F_B - \delta \kappa^{*T} M_B\right] + \int_{t_1}^{t_2} \int_0^l \overline{\delta W} dt = \overline{\delta A} \tag{5}$$

where the superscript * means that the specific terms must satisfy the geometrically exact equations in a frame. The geometrically exact equations are

$$\begin{aligned} \gamma^* &= C^{Ba}\left(C^{ab} e_1 + U_a'\right) - e_1 \ , & \kappa^* &= C^{ba}\left\{\frac{\Delta - \frac{\tilde{\theta}}{2}}{1 + \frac{\theta^T \theta}{4}}\right\} \theta' \\ V_B^* &= C^{Ba}\left(\nu_a + \dot{u}_a + \tilde{\omega}_a u_a\right) \ , & \Omega_B^* &= C^{ba}\left(\frac{\Delta - \frac{\tilde{\theta}}{2}}{1 + \frac{\theta^T \theta}{4}}\right) \dot{\theta} + C^{Ba} \omega_a \end{aligned} \tag{6}$$

where u_a is the displacement vector measured in the a frame, θ is the rotation vector expressed in terms of Rodrigues parameters. The Rodrigues parameters are defined in terms of a rotation of magnitude about a unit vector, $e = e_i b_i$, as $\theta_i = 2e_i \tan(\alpha/2)$. Δ is the 3×3 identity matrix, ν_a and u_a are the initial velocity and initial angular velocity of a generic point on the a frame, and e_1 is the vector $[1\ 0\ 0]^T$.

The rotation matrix, $C = C^{ab} C^{Ba}$ is expressed in terms of the rotation parameter, θ, as follows

$$C = \frac{\left(1 - \frac{\theta^T\theta}{4}\right)\Delta - \tilde{\theta} + \frac{\theta\theta^T}{2}}{1 + \frac{\theta^T\theta}{4}} \tag{7}$$

where $\tilde{\theta}$ operator converts θ to its dual matrix.

The Lagrange multipliers are used to enforce the satisfaction of the kinematical equations. The a frame version of the complete variational formulation, based on an exact intrinsic equation for dynamics of moving beams is described in detail in Shang [7].

Generalized Greenberg's aerodynamic model

Aerodynamic analysis for case I is based on the derivation of Dinyavari. This is a generalized version of Greenberg's theory [8] of the incompressible, finite-time, arbitrary motion airfoil theories, suitable for coupled flap-lag-torsional aeroelastic analysis of the rotary blade. The generalized aerodynamic loads consist of two parts: 1) circulatory loads that involve the augmented states as well as the blade dynamics, and 2) noncirculatory loads that involve only the blade dynamics.

$$\begin{aligned}
\overline{L}_{NC} &= \left[\frac{L_{NC}}{a_i \rho_A (bR)(\Omega l)^2}\right] = \left(\frac{b\overline{R}}{2}\right)\left\{\overline{U_y}''(\theta_G^* + \phi^*) - \overline{U_Z}'' - b\overline{R}(\overline{x}_A - 1/2)(\theta_G^{**} + \phi^{**}) + \overline{U_y^*}''(\theta_G + \phi)\right\} \\
\overline{L}_C &= \left[\frac{L_c}{\rho_A a_i (bR)(\Omega l)^2}\right] = [1/2 + H(\psi)]\overline{U}_y''\,\overline{Q} \\
\overline{M}_{NC} &= \left[\frac{M_{NC}}{a_i \rho_A (bR)^2 (\Omega l)^2}\right] = \left(\frac{b\overline{R}}{2}\right)\left\{(\overline{x}_A - 1\overline{U}_y''(\theta_G^* + \phi^*) - (\overline{x} - 1/2)\overline{U}_A^* + (\overline{x}_A - 1/2)\overline{U}_y^{*\prime\prime}\right. \\
&\quad \left. + (\overline{x}_A - 1/2)\overline{U}_y^{*\prime\prime}(\theta_G + \phi) - b\overline{R}(3/8 + \overline{x}_A^2 - \overline{x}_A)(\theta_G^{**} + \phi^{**})\right\} \\
\overline{M}_C &= \left[\frac{M_C}{\rho_A a_i (bR)^2 (\Omega l)^2}\right] = \overline{x}_A \overline{L}_C = \overline{x}_A [1/2 + H(\psi)]\overline{U}_y''\,\overline{Q}
\end{aligned} \tag{8}$$

where x_0 is the location of typical section in spanwise direction of the deformed coordinate, e is the hinge offset, μ is the advance ratio, ψ is an azimuth angle, ζ is lag angle, β is flapping angle, β_p is precone angle, θ_G is total geometric pitch angle from feathering angle, ϕ is torsional elastic deformation of the blade, bR is half chord of the blade, x_A is the aerodynamic center offsets from the elastic center, $\overline{(\ )}$ means non-dimensionalized value, and $(\ )^*$ is $\partial/\partial\psi$. U'' is the velocity at the blade elastic center, and can be expressed as

$$\begin{aligned}
\overline{U}_y'' &= [(\overline{x}_0 + \overline{e}) + \mu\overline{R}sin\psi + \overline{x}_0\zeta^* + \mu\overline{R}sin\psi\zeta] \\
\overline{U}_z'' &= [\overline{R}\lambda + \overline{x}_0\beta^* + (\mu\overline{R}cos\psi + \overline{x}_{0\zeta})(\beta_p + \beta)] \\
\overline{Q} &= [\overline{U}_y''(\theta_G + \phi) - \overline{U}_z'' + b\overline{R}(1 - \overline{x}_A)(\theta_G^* + \phi^*)]
\end{aligned} \tag{9}$$

$H(\psi)$ is the lift deficiency function which is a function of the augmented states. The augmented states are used to convey information regarding the unsteady wake. 3/4-span location

is selected as the typical section for the augmented states because which represents good average for the phase and amplitude of the lift deficiency function for the entire blade. The expression for the lift deficiency function in terms of the augmented states is

$$H(\bar{X}_{TS1}, \bar{X}_{TS2}, \bar{Q}_{TS}: \psi) = \frac{\left[0.006825\left(\frac{\bar{U}_{TS0}}{b\bar{R}}\right)^2\right]\bar{X}_{TS1} + \left[0.10805\left(\frac{\bar{U}_{TS0}}{b\bar{R}}\right)\right]\bar{X}_{TS2}}{\bar{Q}_{TS}} \tag{10}$$

where,

$$\begin{aligned} &\bar{Q}_{TS} = \bar{Q} \qquad evalulated\ at\ \ \bar{x}_0 = \bar{x}_{TS} \\ &\bar{U}_{TS0} = \bar{x}_{TS} + \bar{e} \\ &\begin{Bmatrix} \bar{X}_1^*(t) \\ \bar{X}_2^*(t) \end{Bmatrix} = \begin{bmatrix} 0 & 1 \\ -0.01365(\bar{U}_{T0}/b\bar{R})^2 & -0.3455(\bar{U}_{T0}/b\bar{R}) \end{bmatrix} \begin{Bmatrix} \bar{X}_1(t) \\ \bar{X}_2(t) \end{Bmatrix} + \begin{Bmatrix} 0 \\ \bar{Q}_{TS} \end{Bmatrix} \end{aligned} \tag{11}$$

Now consider a hovering flight assuming a constant inflow. Then the advance ratio becomes $\mu = 0$, cyclic pitch angle change also $\theta_G^* = 0$, and thus the inflow ratio change will be $\lambda^* = 0$. When there exists a linear pretwist in the blade, the total geometrical pitch angle becomes a function of x_0, $\theta_G(\bar{x}_0) = \theta_0 + \kappa\bar{x}_0$.

It is finally required to transform the airloads equations in the undeformed coordinate to the global a coordinate system, f_a, m_a. Simple transformation matrix can be used for this as follows.

$$\begin{bmatrix} 1 & -\zeta & \beta \\ \beta\phi & 1 & \phi \\ \beta - \zeta\phi & -\zeta\beta - \phi & 1 \end{bmatrix} \tag{12}$$

Unsteady panel method

The aerodynamic model for case II is based on the unsteady source-doublet panel method coupled with a free wake model. Its original model is developed to estimate the time-dependent performance of the rotors, propellers, and general aerodynamic surfaces in various flight conditions. One advantage of the source-doublet panel method is that it is capable of considering the thickness of the rotor blade, while the lifting line method and vortex lattice are not. This results in more exact representation of the blade geometry.

If the flow in the fluid region is considered to be incompressible and irrotational, then the continuity equation reduces to Laplace's equation.

$$\nabla^2 \Phi = 0 \tag{13}$$

The general solution of Eq. (13) is given as a sum of source and doublet distribution over the body's surface and its wakes.

$$\Phi(\vec{P}) = \frac{-1}{4\pi}\int_{body}\left[\sigma\left(\frac{1}{r}\right) - \mu\vec{n} \cdot \nabla\left(\frac{1}{r}\right)\right]ds + \frac{1}{4\pi}\int_{wake}\left[\mu\vec{n} \cdot \nabla\left(\frac{1}{r}\right)\right]ds + \Phi_\infty(\vec{P}) \tag{14}$$

However, Eq. (14) still does not uniquely describe a solution since a large number of source and doublet distributions exist to satisfy a set of boundary conditions. To determine a unique solution, the source distribution is set to be equal to the local kinematic velocity as in PMARC. The source strength becomes

$$\sigma = -\hat{n} \cdot (\vec{V_0} + \vec{\nu}_{rel} + \vec{\Omega} \times \vec{r}) \tag{15}$$

In order to establish the boundary value problem, the local velocity at each panel on the body has to satisfy the zero flow condition across the body surface.

$$\nabla\Phi \cdot \hat{n} - \overrightarrow{V_f} \cdot \hat{n} = 0 \tag{16}$$

Also, from the Kutta condition, the latest wake doublets are expressed in terms of the unknown surface doublets.

$$\mu_{wake} = \mu_{T.Eupper} - \mu_{T.Elower} \tag{17}$$

When specified at the body's N collocation points, Eq. (17) will have the form

$$[A_{ij}](\mu_k) = (RHS_k) = [B_{ij}](\sigma_k) + [C_{ij}](\mu_{wk}) \tag{18}$$

This matrix has a nonzero diagonal and has a stable numerical solution. The resulting pressures can be computed by Bernoulli equation, which yields

$$C_p = -\frac{(\nabla\Phi)^2}{\nu_{ref}^2} + \frac{2}{\nu_{ref}}[\overrightarrow{V_0} + \overrightarrow{\Omega} \times \vec{r}] \cdot \nabla\Phi - \frac{2}{\nu_{ref}}\frac{\partial\Phi}{\partial t} \tag{19}$$

The contribution of an element with an area of ΔS_k to the aerodynamic loads ΔF_k is given as follows.

$$\Delta F_k = -C_{pk}\left(\frac{1}{2}\rho\nu_{ref}^2\right)_k \Delta S_k \vec{n}_k \tag{20}$$

To take the wake effects into consideration with accuracy, the present source-doublet panel method is combined with the time-marching free wake model. For a better wake rollup simulation, the wake doublet panel with constant strength is substituted with an equivalent vortex ring [9]. The singularity problem in the vortex center is treated by Vatitas's vortex model [10].

$$\vec{V} = \frac{\Gamma}{2\pi}\frac{h}{(r_c^{2n} + h^{2n})^{1/n}}(\cos\theta_1 - \cos\theta_2)\vec{e} \tag{21}$$

where n is integer (Fig. 2).

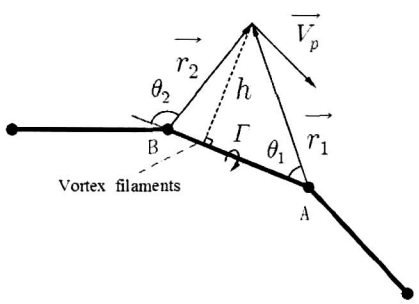

Fig. 2. Schematic showing the velocity induced by a straight-line vortex element

Validation on the second aerodynamic model in itself is conducted by comparing with the experimental data upon a full-scale propeller and a model helicopter rotor in hover [11, 12]. As in Figs. 3 and 4, the numerical results from the present aerodynamic model are found to be in good agreement with experimental data. The converged aerodynamic forces and moments are usually obtained after 10 rotor revolutions including initial slow start (2 rotor rev.). The geometry of the rotor and wake is illustrated in Fig. 5 after 10 revolutions. The lines represent the tip vortex and the scattered points show the edge points of the inner wake panels. The trajectories of the tip vortices are also shown in Fig. 6. The results of the present model show good agreement in terms of the radial and downstream distance positions.

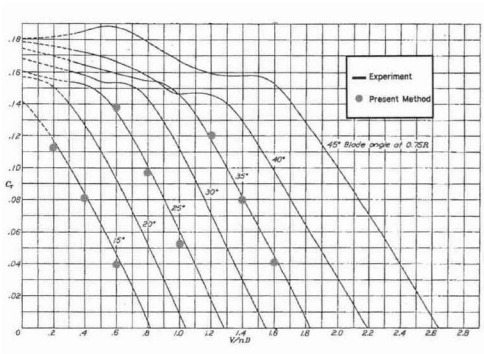

Fig. 3. Thrust coefficient for Propeller 5808-9, Clark Y, 3 Blades

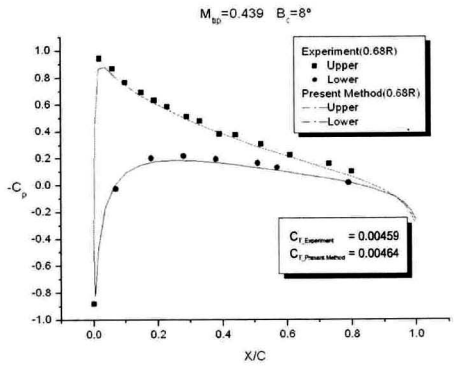

Fig. 4. Comparison of the pressure distribution

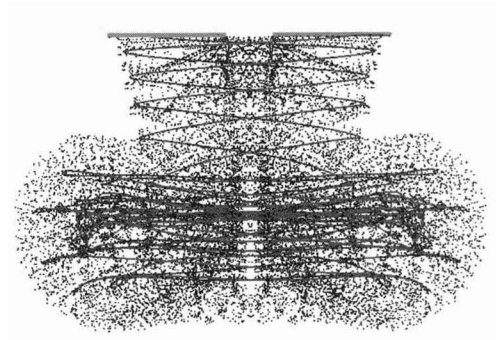

Fig. 5. Wake geometry of the hovering rotor

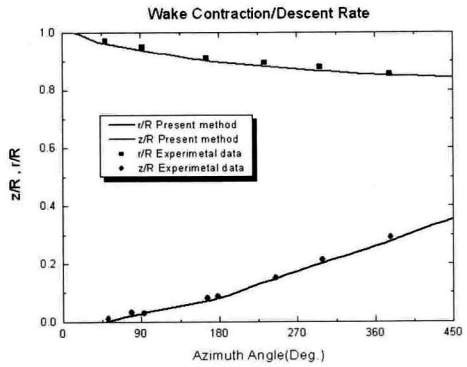

Fig. 6. Wake contraction/descent rate

Finite element discretization and the governing equations for CASE I model

By discretizing the blade into N elements, the structural and finite-time aerodynamic equations can be rewritten in the following form:

$$\int_{t_1}^{t_2} \sum_i \delta \Pi_i dt = 0 \tag{22}$$

where index i indicates an ith element with length Δl_i, and $\delta \Pi_i$ is the corresponding spatial integration over the ith element. The simplest shape functions can be used in this form, and the effective nodal airload vectors can be obtained using the following relations

$$\begin{aligned} \bar{f}_i &= \int_{l_i} (1-\xi) f_a dx_1 \quad , \quad \bar{f}_{i+1} = \int_{l_i} \xi f_a dx_1 \\ \bar{m}_i &= \int_{l_i} (1-\xi) m_a dx_1 \quad , \quad \bar{m}_{i+1} = \int_{l_i} \xi m_a dx_1 \end{aligned} \tag{23}$$

Once discretization is accomplished on the structural and aerodynamic part, the resulting equations can be expressed in a simple form as follows.

$$F_S(X, \dot{X}) - F_L(X, \dot{X}) = 0 \tag{24}$$

where F_S is the structural operator, F_L is the airload operator, and X is the unknown vector consisting of structural variables in the following form:

$$X = [\hat{F}_1^T \ \hat{M}_1^T \ u_1^T \ \theta_1^T \ F_1^T \ M_1^T \ P_1^T \ H_1^T \ \cdots \ u_N^T \ \theta_N^T \ F_N^T \ M_N^T \ P_N^T \ H_N^T \ \hat{u}_N^T \ \hat{\theta}_N^T]^T \tag{25}$$

Structural variables in (24) can be further expressed in the following form:

$$X = \bar{X} + \check{X}(t) \tag{26}$$

where $\bar{X}$ is the steady component of the solution, which is independent of time, and $\check{X}(t)$ is the transient component of the solution, or, the perturbed motion, which has time dependency.

In the steady state, $\check{X}(t) = 0$, therefore the governing equations can be simply written as

$$F_S(\bar{X}) - F_L(\bar{X}) = 0 \tag{27}$$

Since the pertinent operators have explicit expressions, the Jacobian matrix can then be derived by differentiation:

$$[J] = \left[\frac{\partial F_S}{\partial \bar{X}} - \frac{\partial F_L}{\partial \bar{X}} \right] \tag{28}$$

whose detailed expressions for the structural part are listed in [6].

Equation (27) can be calculated by Newton-Raphson method, and this solution will be used as a initial for time integration calculation.

To deal with time-derivative terms, a second-order backward Euler method is adopted. The following finite difference discretization scheme is applied at each time step, n:

$$\dot{X}_i^n = \frac{3X_i^n - 4X_i^{n-1} + X_i^{n-2}}{2\Delta t} \tag{29}$$

where Δt is the time-step size. Superscripts indicate the time step and subscripts are the node index.

Now Equation (24) can be solved using Newton's method. The Jacobian matrix can be derived explicitly by differentiation:

$$[J] = \left[\frac{\partial F_S}{\partial X} - \frac{\partial F_L}{\partial X} \right] \tag{30}$$

whose detailed expressions for the structural part are listed in [13], and those for the aerodynamics can be developed in same way as that of steady case with unsteady aerodynamic terms.

Fluid-structure combination for CASE II model

The aerodynamic module of the source-double panel method is loosely coupled with the structural module, which means that the data from each module are exchanged in an indirect manner. Before the initial transfer of the aerodynamic data, the panel code is converged without any consideration of structural deflection. And detailed coupling procedure is as follows.

1) In every 10 degree of azimuth angle, the forces and moments obtained from aerodynamic analysis module are transferred to the structural analysis module. Because In general, aerodynamic node points are not coincident with structural node points, the aerodynamic forces must be interpolated before transfer. The viscous drag is not calculated in the panel method so that its effects are included by table look-up obtained from experiments.

2) Based on the forces and moments transferred from the aerodynamic module, the structural module calculates the structural defections. The magnitude of deflection and rotation angles are interpolated at each aerodynamic node point.

3) By using the deflection and rotation angles, the aerodynamic surface grid is newly generated.

4) The procedure is repeated until the converged thrust is obtained.

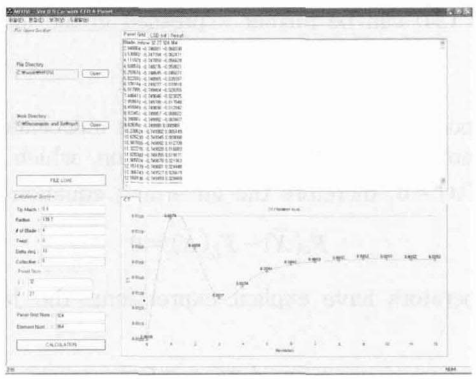

Fig. 7. The automation program of the combining procedure

To automatize this exchange process, a separate interface module is developed as shown in Fig. 7. The interface module is coded based on MFC of Visual C++ so that the data exchange can be easily accomplished. To this end, a unified data format is defined for the data transfer between the analysis modules. The input parameters required for each analysis are directly modified in the GUI module and the calculation results are also shown in the same window.

Results and Discussion

Numerical results of CASE I model

In spite of its model simplicity, the generalized Greenberg's theory has one advantage. By relatively simple representation of the relevant lift deficiency function, it is implemented with ease to incorporate it with structural model. Using the generalized Greenberg's theory, time domain analysis for the hovering flight condition is performed in this paper. The offset-hinged, pre-twisted, articulated, small-scaled experimental rotor blade is examined. Uniform inflow is assumed in the analysis, and it is evaluated from the following relation.

$$\lambda = (\sigma a_i/16)[\sqrt{1+(24\theta_C/\sigma a_i)}-1] \tag{31}$$

The resulting lift force when the rotating speed is linearly increases for the first 1 second, and Fig. 8 shows blade spanwise load distribution. Comparing it with the result from CAMRAD II, the present analysis appears larger by approximately 25%. This is due to the single blade aerodynamic model adopted in this paper. The effects of the returning wake among the multiple blades usually act as damping, and this may decrease overall forces and deformations.

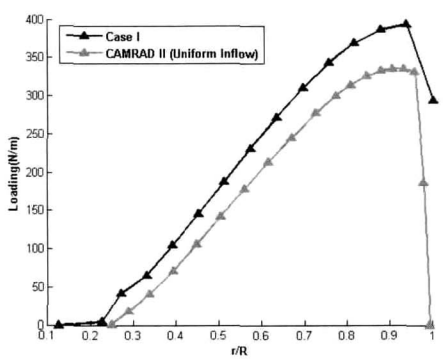

Fig. 8. Blade spanwise loading from case I

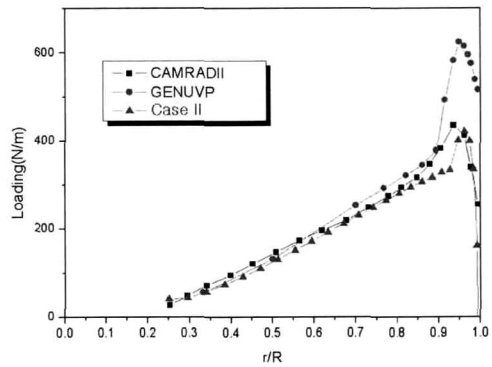

Fig. 9. Blade spanwise loading from case II

Numerical results of CASE II model

Fig. 9 shows the comparative results for the spanwise load distributions of the same small-scaled experimental rotor blade in hover. The present calculation is compared to CAMRAD II and GENUVP [14]. Similar load distribution is observed up to r/R=0.85 but significant discrepancies are found at the tip region, which results from the difference of wake geometry for each analysis. It is seen that the present results are relatively in agreement with those of CAMRAD II but are substantially different from those of GENUVP at the tip region. The computed thrust is 208.006 N, which is about 4% smaller than 216.453 N from CAMRAD II.

Comparison between CASE I and II models

Fig. 10 shows the blade spanwise loading in the opposite direction of the flight. And Figs. 11 and 12 show the flap and lag angle distribution comparison of the two models respectively. Through these two results about the blade deflection, it is possible to evaluate the effect of airloads to blade behaviors.

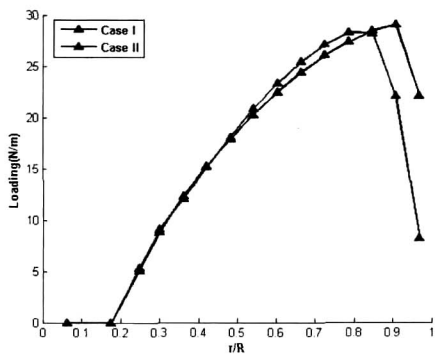

Fig. 10. Blade spanwise loading from case I

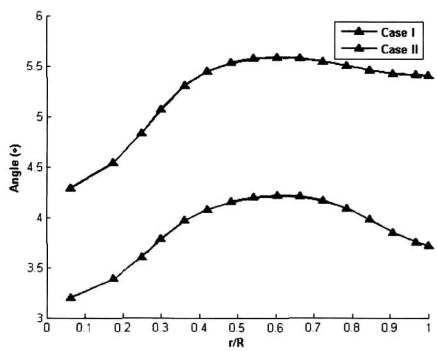

Fig. 11. Blade spanwise flap angle distribution

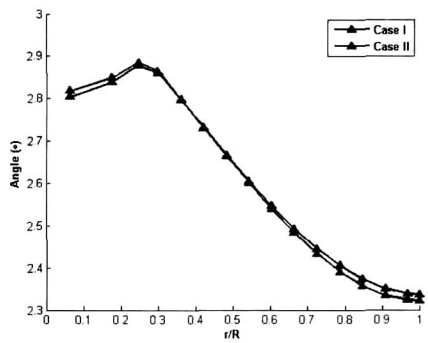

Fig. 12. Blade spanwise lag angle distribution

Conclusions

In this paper, two models which applied a sophisticated structural model using geometrically nonlinear beam theory and different aerodynamics are examined for the calculation of the interaction of the rotorcraft in hovering state. The generalized Greenberg's finite-time aerodynamics is for used for CASE I model, it is explicitly coupled with structure part. The unsteady source-doublet method which is coupled with a free wake model is used for CASE II

model, and it is loosely coupled with structure model. Transient time responses about airloads and blade behavior are examined, and comparison between two models is also conducted.

For the future work, forward flight analysis will be attempted, which includes a trim analysis in both the finite-time aerodynamics and panel method. Also a new finite-time aerodynamic model will be adopted, which considers multiple-blade effects.

Acknowledgement

This work was supported by Grant No. R01-2005-10059-0 from the Basic Research Program of the Korea Science & Engineering Foundation.

References

1. Potsdam, M., Yeo, H., and Johnson, W., "Rotor Airloads Prediction using Loose Aerodynamic/Structural Coupling", American Helicopter Society 60th Annual Forum, Baltimore, MD, Jun., 7-10, 2004.

2. Datta, A., and Chopra, I., "Prediction of UH-60A Dynamic Stall Loads in High Altitude Level Flight using CFD/CSD Coupling" American Helicopter Society 61th Annual Forum, Grapevine, TX, Jun., 1-3, 2005.

3. Shin, S. J., Cesnik, C. E. S., and Hall, S. R., "Closed-Loop Control Test of the NASA/Army/MIT Active Twist Rotor for Vibration Reduction", Journal of the American Helicopter Society, Vol. 50, No. 2, pp. 178-194, 2005.

4. Dinyavari, M. A. H., and Friedmann, P. P., "Application of Time-Domain Unsteady Aerodynamics to Rotary-Wing Aeroelasticity", AIAA Journal, Vol. 24, No. 9, pp. 1424-1432, 1986.

5. Lee, J. W., Yee, K. J., and Oh, S. J., "The Aerodynamic Analysis of Helicopter Rotors by Using an Unsteady Source-Doublet Panel Method", Journal of KSAS, Vol. 34, No. 6, pp. 1-9, 2006.

6. Hodges, D. H., "A Mixed Variational Formulation based on Exact Intrinsic Equations for Dynamics of Moving Beams", International Journal of Solids and Structures, Vol. 25, No. 11, pp. 1253-1273, 1990.

7. Shang, X., "Aeroelastic Stability of Composite Hingeless Rotors with Finite-State Unsteady Aerodynamics", Ph.D. Dissertation, Georgia Institute of Technology, Aug., 1995.

8. Greenberg, J. M., "Airfoil in Sinusoidal Motion in Pulsating Stream", NACA TN 1326, 1947.

9. Hess, J. L., "Calculation of Potential Flow About Arbitrary Three-Dimensional Lifting Bodies," Final Technical Report MDC J5679-02, McDonnell Douglas, Long Beach, California, 1972.

10. Vatistas, G. H., Kozel, V., and Mih, W., "A Simpler Model for Concentrated Vortices", Experiments in Fluids, Vol. 11, pp. 73-76, 1991.

11. Caradonna, F. X. and Tung, C., "Experimental and Analytical Studies of a Model Helicopter Rotor in Hover", NASA-TM 81232, 1981.

12. Hartman, E. P. and Biermann, D., "The Aerodynamic Characteristics of Full-Scale Propellers having 2, 3, and 4 Blades of Clark Y and R. A. F. 6 Airfoil Section", NACA-TR 640, 1937.

13. Cheng, T., "Structural Dynamics Modeling of Helicopter Blades for Computational Aeroelasticity", S.M. Thesis, Massachusetts Institute of Technology, May., 2002.

14. Opoku, D. G., "Aeroelastic and Aeroacoustic Modelling of Rotorcraft", S.M. Thesis, Garleton University, Ottawa, Canada, Sep., 2002.